

# Structure of Dark Matter Halos From Hierarchical Clustering: II. Universality and Self-Similarity in Cluster-Sized Halos

Toshiyuki Fukushige

Department of General Systems Studies,  
College of Arts and Sciences, University of Tokyo,  
3-8-1 Komaba, Meguro-ku, Tokyo 153-8902, Japan

Junichiro Makino

Department of Astronomy,  
School of Sciences, University of Tokyo,  
7-3-1 Hongo, Bunkyo-ku, Tokyo 117-0033, Japan

## ABSTRACT

We investigate the structure of the dark matter halo formed in three different cold dark matter scenarios. We performed N-body simulations of formation of 13 cluster-sized halos. In all runs, density cusps proportional to  $r^{-1.5}$  developed at the center. This result was independent of the cosmological models we simulated. We could not reproduce the cusp shallower than  $r^{-1.5}$ , which was obtained in some of previous studies. We also found that in all runs the density structure evolves in a self-similar way, even in  $\Omega \neq 1$  universes. These results show that the formation of structural form is a process decoupled from a background cosmology.

*Subject headings:* cosmology:theory — dark matter — galaxies: clusters: general — methods: N-body simulations

## 1. Introduction

The structure of dark matter halos formed through dissipationless hierarchical clustering from cosmological initial setting has been explored by many researchers since the "finding" of the universal profile by Navarro, Frenk and White (1996, 1997, hereafter NFW). NFW performed  $N$ -body simulations of the halo formation and found that the density profiles of dark matter halos were expressed well by a simple formula,

$$\rho = \frac{\rho_0}{(r/r_0)(1 + r/r_0)^2} \quad (1)$$

where  $\rho_0$  is a characteristic density and  $r_0$  is a scale radius. They argued that the profile of dark matter halos have the same shape, independent of the halo mass, the initial density fluctuation spectrum or the value of the cosmological parameters.

Although the NFW results have been confirmed regarding the logarithmic slope shallower than isothermal near the center and  $-3$  in the outskirts, disagreements concerning the slope of the central region were reported by subsequent studies in which higher-resolution simulations were performed. The disagreements are summarized into the following two kinds.

One is that the slope at the center is steeper than that in the NFW result. Fukushige and Makino (1997, hereafter FM97) performed a simulation with 768k particles, while previous studies employed  $\sim 20k$ , and found that the galaxy-sized halo in their simulation has a cusp steeper than  $\rho \propto r^{-1}$ . Moore et al. (1998, 1999 hereafter M99) and Ghigna et al. (2000) performed simulations with up to 4M particles and obtained the results that the profile has a cusp proportional to  $r^{-1.5}$  both in galaxy-sized and cluster-sized halos. They proposed the modified universal profile (hereafter, the M99 profile),

$$\rho = \frac{\rho_0}{(r/r_s)^{1.5}[1 + (r/r_s)^{1.5}]} \quad (2)$$

Klypin et al. (2001) also obtained the results the the slope at the center can be approximated by  $r^{-1.5}$ , though they argued that the NFW fit is still good up to their resolution limit.

The second is that the slope at the center is not universal. Jing and Suto (2000) performed a series of  $N$ -body simulations and concluded that the power of the cusp depends on mass, in contradiction to the claims by earlier studies. It varies from  $-1.5$  for galaxy mass halo to  $-1.1$  for cluster mass halo. Also, many analytical studies argued that the halo profile should depend on the power spectrum of initial density fluctuation. For example, Hoffman and Shaham (1985) and Syer and White (1998) predicted the slope,  $3(n+3)/(n+4)$  and  $3(n+3)/(n+5)$ , respectively, where  $n$  is the effective power-law index of the power spectrum.

In the first paper of this series (Fukushige and Makino 2001, hereafter Paper I), we performed simulations of 12 halos with the mass ranging from  $6.6 \times 10^{11} M_\odot$  to  $8.0 \times 10^{14} M_\odot$ . We found that, in all runs, the halos have density cusps proportional to  $r^{-1.5}$  developed at the center. This result means that the density structure is universal in the sense that it is independent of the halo mass. We also found that the density structure evolves in a self-similar way as the central cusp grows outward with keeping the density near the center unchanged.

This paper is a follow up of Paper I. In this paper, we focus on the dependence

of the halo profile on the cosmological model. We simulate halos in three conventional cold dark matter models: Standard, Lambda and Open CDM models, while simulations in Paper I was performed only in the standard CDM model. We performed  $N$ -body simulations of formation of 13 cluster-sized dark matter halos using Barnes-Hut treecode and a special-purpose computer GRAPE-5 (Kawai et al. 2000). This is the first study that investigates the dependence on the different CDM models with the mass resolution and number of samples enough to discuss the slope of the cusp, though several simulations were performed in the same context (NFW, Thomas et al. 1998, Huss, Jain, and Steinmetz 1999).

The structure of this paper is as follows. In section 2, we describe the model of our  $N$ -body simulation. In section 3, we present the results of simulation. Section 4 is for conclusion and discussion.

## 2. Simulation Method

We simulated the formation of the dark matter halos using "re-simulation" method, which has been the standard method for the simulation of halo formation since NFW. In this method, we first perform large scale cosmological simulations in order to identify the halo candidates. We trace back to the initial condition of the large scale simulation, and express the halo candidate with larger number of particles by adding a shorter wavelength perturbation. Then, we resimulate the halo candidates.

We used three cosmological models listed in Table 1: Standard, Open and Lambda Cold Dark Matter models (SCDM, OCDM, and LCDM). Here,  $\Omega_0$  is the density parameter,  $\lambda_0$  is the dimensionless cosmological constant,  $H_0 = 100h \text{ km} \cdot \text{s} \cdot \text{Mpc}^{-1}$  at the present epoch, and  $z_i$  is the initial redshift. The amplitudes of the power spectrum in CDM models were normalized using the top-hat filtered mass variance at  $8h^{-1} \text{ Mpc}$  according to the cluster abundance (Kitayama & Suto 1997).

The large scale cosmological simulations were performed with  $1.1 \times 10^6$  particles in a sphere of 100Mpc radius. The procedure for setting the initial condition were the same as those used in Fukushima and Suto (2001). We regard a spherical overdensity region around a local potential minimum within  $r_v$  as a candidate halo. We define the radius  $r_v$  such that the spherical overdensity inside is  $178\Omega_0^{0.3}$  times the critical density for SCDM and OCDM model, and  $178\Omega_0^{0.4}$  times for LCDM model (Eke, Cole, Frenk 1996).

We selected 13 halos from the candidate halos catalog, which are summarized in Table 2. We first selected the most massive halo in each CDM model, and then selected the halos

at random from halo candidates containing more than 1000 particles. We expressed a region within  $5r_v$  from the center of the halo at  $z = 0$  in the cosmological simulation with larger number of particles. We placed particles whose mass is the same as that in the cosmological simulation in a sphere of  $\sim 50\text{Mpc}$  radius surrounding the high resolution region in order to express the external tidal field. The total number of particles,  $N$ , is listed in Table 2. As a result, the mass ratio between the high resolution particles and surrounding particles becomes rather large,  $256 \sim 2048$ . In order to prevent the contamination of heavy particles into the halo, we set the boundary to be a rather large value,  $5r_v$ . No heavy particle entered within  $r_v$  throughout all simulations.

We integrated the system directly in the physical coordinates for both the cosmological and halo simulations (as in FM97, Paper I). We used a leap-frog integrator with shared and constant timestep. The step size for the cosmological simulation is  $\Delta t/t_H = 1/1024$  and that for the halo simulation is listed in Table 2. The code for the time integration is the same as that in Fukushige and Suto (2001). We used the usual Plummer softening. The gravitational softening  $\varepsilon$  is constant in the physical coordinates and the length is 5kpc for the cosmological simulation and 1kpc for all halo simulations.

The force calculation is done with the Barnes-Hut tree code (Barnes & Hut 1986, Makino 1991) on GRAPE-5 (Kawai et al. 2000), a special-purpose computer designed to accelerate  $N$ -body simulations. For most simulations, we used the GRAPE-5 system at the Astronomical Data Analysis Center of the National Astronomical Observatory, Japan. We used the opening parameter  $\theta = 0.4$  for the cosmological simulation and  $\theta = 0.5$  for the halo simulation. The simulations presented below required, for example in Run L6,  $\sim 80$  secs per timestep, and thus one run (16k timesteps) was completed in 370 CPU hours with a GRAPE-5 board connected to a host workstation with Alpha 21264 CPU (833MHz).

Table 1: Cosmological Models

Model	$\Omega_0$	$\lambda_0$	$h$	$\sigma_8$	$\rho_{\text{crit}}(M_\odot/\text{pc}^3)$	$z_i$
SCDM	1.0	0.0	0.5	0.6	$6.9 \times 10^{-8}$	24.0
LCDM	0.3	0.7	0.7	1.0	$1.4 \times 10^{-7}$	32.3
OCDM	0.3	0.0	0.7	1.0	$1.4 \times 10^{-7}$	32.3

### 3. Results

### 3.1. Snapshots

Figure 1 shows the particle distribution for all runs at  $z = 0$ . The length of the side for each panel is equal to  $2r_v$ . For these plots, we shifted the origin of coordinates to the position of the potential minimum. In Table 2, we summarized the radius  $r_v$ , the mass  $M_v$ , and the number of particles  $N_v$  within  $r_v$  at  $z = 0$ .

### 3.2. Density Profile

Figure 2 shows the density profiles for all runs at  $z = 0$ . For Run O2, we plot the density profile at  $z = 0.026$  because the merging process occurs just near the center of halo at  $z = 0$ . The position of the center of the halo was determined using the potential minimum and the density is averaged over each spherical shell whose width is  $\log_{10}(\Delta r) = 0.0125$ . For the illustrative purpose, the densities are shifted vertically.

In this figure, we plot the densities in the thick lines if the two criteria introduced in Paper I; (1)  $t_{\text{rel}}(r)/t > 3$  and (2)  $t_{\text{dy}}(r)/\Delta t > 40$ , are satisfied, where  $t_{\text{rel}}(r)$  is the local two-body relaxation time and  $t_{\text{dy}}(r)$  is the local dynamical time. This means that the densities in the central region plotted in the thin lines are influenced by the numerical artifacts (mainly two-body relaxation), and they are not reliable. In the following discussion, we only use the densities plotted in the thick lines.

In all runs we can see the central density cusps approximately proportional to  $r^{-1.5}$ . In other words, the power of the cusp is  $-1.5$  and is independent of cosmological models we simulated. The shallowing of the power-law index of the inner cusp observed in the LCDM runs by Jing and Suto (2000) was not reproduced in our LCDM runs.

Moreover, the density profiles are in good agreement to the profile given by equation (2) (the M99 profile) in all runs. We set the scale radii  $r_0$  as 0.8, 0.5, 0.4, 0.5 Mpc for S1..S4 runs, 0.6, 0.5, 0.5, 0.35, 0.3, 0.3 Mpc for L1..L6 runs, and 0.35, 0.35, 0.25 Mpc for O1..O3 runs. The agreement is very good for the inner region. In the outer region the agreement is not very good simply because the outer profile shows large fluctuations caused by individual infalling halos. The degree of the agreement is better in LCDM and OCDM model than in SCDM model. This is because the halo in LCDM and OCDM model is typically formed earlier and it is dynamically quiet around  $z \sim 0$ .

Figure 3 shows the scale densities of the profile  $\rho_0$  [equation (2)] and the concentration parameter  $c \equiv r_v/r_0$  as a function of total mass. These values in S/LCDM models are consistent to those obtained by M99 and Jing and Suto (2000). We can see a tendency that

that cluster-size halos in OCDM models are more compact than that of their S/LCDM counterparts of the same mass.

### 3.3. Self-Similarity

In the SCDM simulations of Paper I, we found that the density profile evolves in a self-similar way as the central cusp grows outward keeping the density near the center unchanged (illustrated in Figure 14 of Paper I). However, it is not clear whether the density profile evolves in the same way in the LCDM and OCDM model, because neither of models retains the scale-free nature of the SCDM model.

If the evolution is self-similar, we can write the density as

$$\rho(r, t) = \rho_{\dagger}(M)\rho_*(r_*) \quad (3)$$

$$r_* = r/r_{\dagger}(M) \quad (4)$$

In Paper I, we obtained the self-similar variables,  $\rho_{\dagger}$  and  $r_{\dagger}$ , as

$$\rho_{\dagger}(M) = \left( \frac{M}{10^{14}M_{\odot}} \right)^{\frac{n}{3+n}} \quad (5)$$

$$r_{\dagger}(M) = \left( \frac{M}{10^{14}M_{\odot}} \right)^{\frac{1}{3+n}} \quad (6)$$

assuming that the halo having a  $r^n$  cusp grows outward in a self-similar way keeping the density of central cusp region constant and the fraction of mass in the cusp to total mass,  $M$ , is constant. Here  $n$  is the power of the cusp.

In Figure 4 we plot the scaled density  $\rho_*$  as a function of  $r_*$ . We plot three profiles at different value of the redshifts  $z$  for six runs. We set  $n$  to be  $-1.5$  and use  $M_v$  as the total mass. In this figure, we can see that the density profiles of the same halo at different times show good agreement to each other, which means that the density structure evolves self-similarly. Therefore, Figure 4 demonstrates that our assumption of the self-similarity is justified not only in the SCDM model, but also in LCDM and OCDM models.

Finally, we consider whether halos of different masses are on the self-similar evolution track or not. If a halo evolves self-similarly, scaled scale densities  $\rho_{*0} \equiv \rho_0/\rho_{\dagger}$  should be constant during the evolution. Using equation (5), the scale density  $\rho_0$  is proportional to  $M^{-1}$ . In Figure 3, the dashed line indicates  $\rho_0 \propto M^{-1}$ . If the halo evolve self-similarly, the evolution track is along the dashed line in the  $\rho_0 - M$  plot. We can see a tendency that at least for O/LCDM models, halos do not distribute along the self-similar evolution track, in other words, small halos cannot grow to large halos even if we wait longer.

#### 4. Conclusion and Discussion

We performed  $N$ -body simulations of dark matter halo formation in three CDM models: Standard, Lambda, and Open CDM models. We simulated 13 halos whose mass range is  $1.8 \times 10^{14} M_{\odot}$  to  $8.6 \times 10^{14} M_{\odot}$ . We used a widely adapted "re-simulation" method to set up initial conditions of halos and include the external tidal field.

Our main conclusions are:

- (1) We found that, in all runs, the final halos have density cusps proportional to  $r^{-1.5}$ , and the profiles show good agreement with the M99 profile, regardless of the cosmological models.
- (2) In all runs, the density profile evolves self-similarly. This is also independent of the cosmological models we simulated.

There are some claims that the innermost slope should converge not to  $r^{-1.5}$  but to a shallower one (e.g. Taylor, Navarro 2001). Indeed, if we do not pay attention to numerical artifacts, we may see in our simulation results (Figure 2) that the innermost slopes of all runs become shallower than  $-1.5$ . However, Figure 2 shows that the inner region where the slope are shallower than  $r^{-1.5}$  is not reliable because in this region the accuracy criteria are not satisfied. The numerical artifact which makes the cusp shallower is mainly the two-body relaxation effect in this region (see Paper I). Therefore, we emphasize that discussions based on simulation results without careful analysis of the influence by the two-body relaxation effects are misleading.

In our LCDM run, we could not reproduce the shallowing of the power-law index of the inner cusp observed in the LCDM runs by Jing and Suto (2000). This difference could be due to the smoothing by two-body relaxation in their cluster-sized halos. In this paper, we show that the density profile within  $\sim 0.01r_{200}$  smoothed by the two-body relaxation. The density at  $0.01r_{200}$  and the mass resolution in their cluster-sized halo are similar to those in ours. The density profile in their simulations within  $0.01r_{200}$ , at which the profile begins to depart from  $r^{-1.5}$  inward, could be affected by the two-body relaxation. If their simulations had been performed with higher mass resolution, the slope might have approach to  $-1.5$ . The tendency can be already seen in their galaxy-sized halo. All halos have the cusp proportional to  $r^{-1.5}$  in their galaxy-sized halos whose central densities at  $0.01r_{200}$  are almost similar to those of their cluster-sized run and mass resolutions are about 100 times higher.

Our results show that the NFW's claim concerning to the universality is certainly

valid. On the other hand, the density profile obtained are not in agreement with the NFW profile at the central region. Although it is important to find the convergence slope by further simulations, a simple explanation would be required for our final understanding of the universal profile. At present, we don't fully understand why the profile is universal and/or why the power of central cusp is  $-1.5$ , which we will address it in the future study.

We are grateful to Atsushi Kawai and Eiichiro Kokubo for their helps in preparing the hardware and software environment of the GRAPE-5 system, and to Yasushi Suto, Atsushi Taruya, and Masamune Oguri for many helpful discussions. We gratefully acknowledge the use of the initial condition generator in the publicly available code *Hydra* (1995) developed by H.M.P.Couchman, P.A.Thomas, and F.R.Pearce. Most of numerical computations were carried out on the GRAPE system at ADAC (the Astronomical Data Analysis Center) of the National Astronomical Observatory, Japan. This research was partially supported by the Research for the Future Program of Japan Society for the Promotion of Science, grant no. JSPS-RFTP 97P01102.

## REFERENCES

- Barnes, J. E., & Hut, P. 1986, *Nature*, 824, 446
- Couchman, H. M. P., Thomas, P. A., & Pearce, F. R. 1995, *ApJ*, 452, 797
- Eke, V. R., Cole, S., & Frenk C. S. 1996, *MNRAS*, 282, 263
- Fukushige, T., & Makino, J. 1997, *ApJ*, 477, L9
- Fukushige, T., & Makino, J. 2001, *ApJ*, in press (Paper I)
- Fukushige, T., & Suto, Y. 2001, *ApJL*, in press
- Ghigna, S., Moore, B., Governato, F., Lake, G., Quinn, T., & Stadel, J. 2000, *ApJ*, 544, 616
- Hoffman, Y., & Shaham, J. 1985, *ApJ*, 297, 16
- Huss, A., Jain, B., & Steinmetz, M. 1999, *MNRAS*, 308, 1011
- Jing, Y. P., & Suto, Y. 2000, *ApJ*, 529, L69
- Kawai, A., Fukushige, T., Makino, J., & Taiji, M. 2000, *PASJ*, 52, 659
- Kitayama, T., & Suto, Y. 1997, *ApJ*, 490, 557
- Klypin, A., Kravtsov, A. V., Bullock, J. S., & Primack, J. R. 2001, *ApJ*, 554, 903
- Makino, J. 1991, *PASJ*, 43, 621
- Moore, B., Governato, F., Quinn T., Statal, J., & Lake, G. 1998, *ApJ*, 499, L5



- Moore, B., Quinn T., Governato, F., Statal, J., & Lake, G. 1999, MNRAS, 310, 1147  
Navarro, J. F., Frenk, C. S., & White, S. D. M., 1996, ApJ, 462, 563  
Navarro, J. F., Frenk, C. S., & White, S. D. M., 1997, ApJ, 490, 493  
Syer, D., & White, S. D. M. 1998, MNRAS, 293, 337  
Thomas, P., et al. 1998, MNRAS, 296, 1061

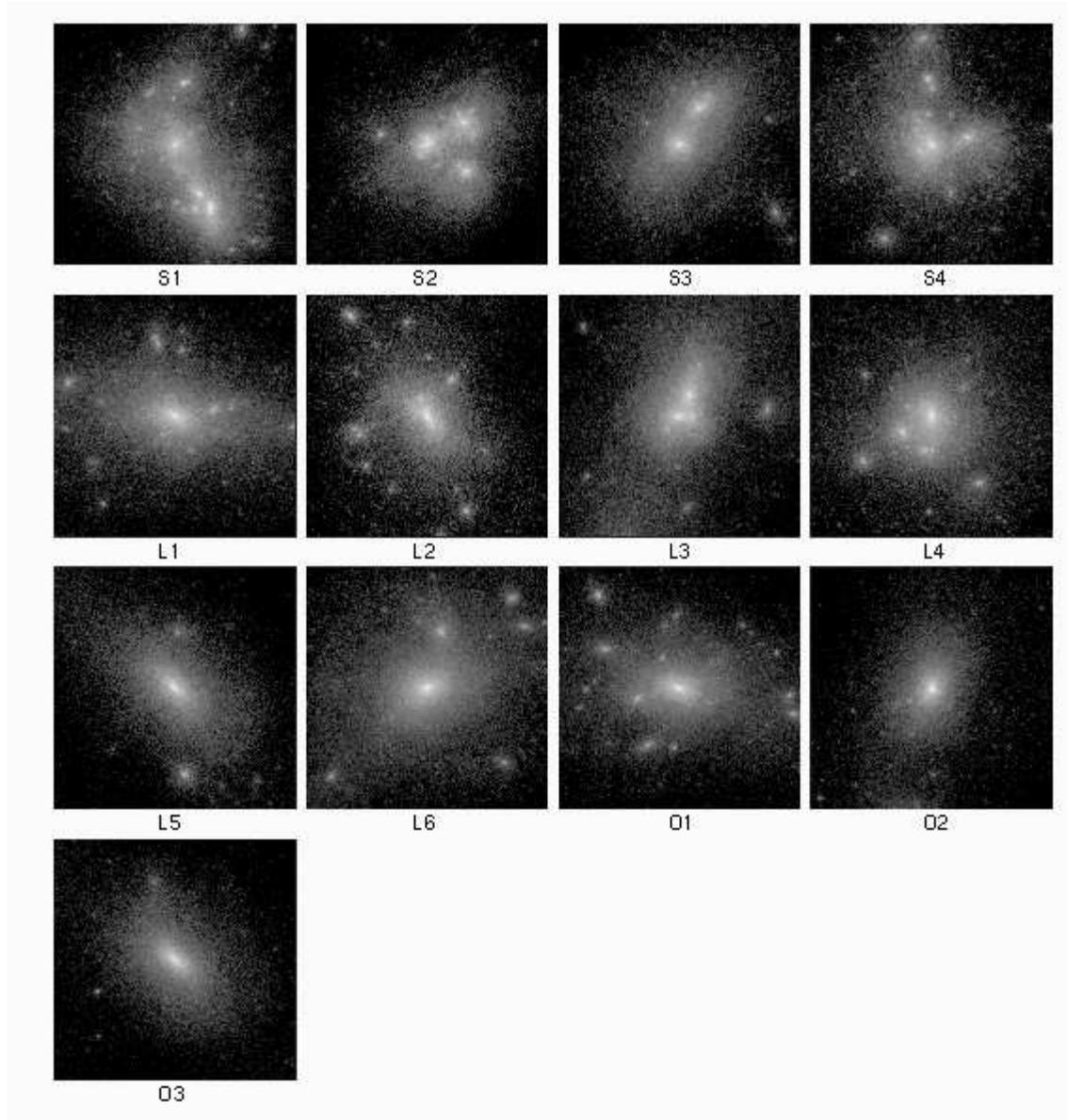


Fig. 1.— Snapshots from all Runs at  $z = 0$ . The length of the side for each panel is equal to  $2r_v$ .

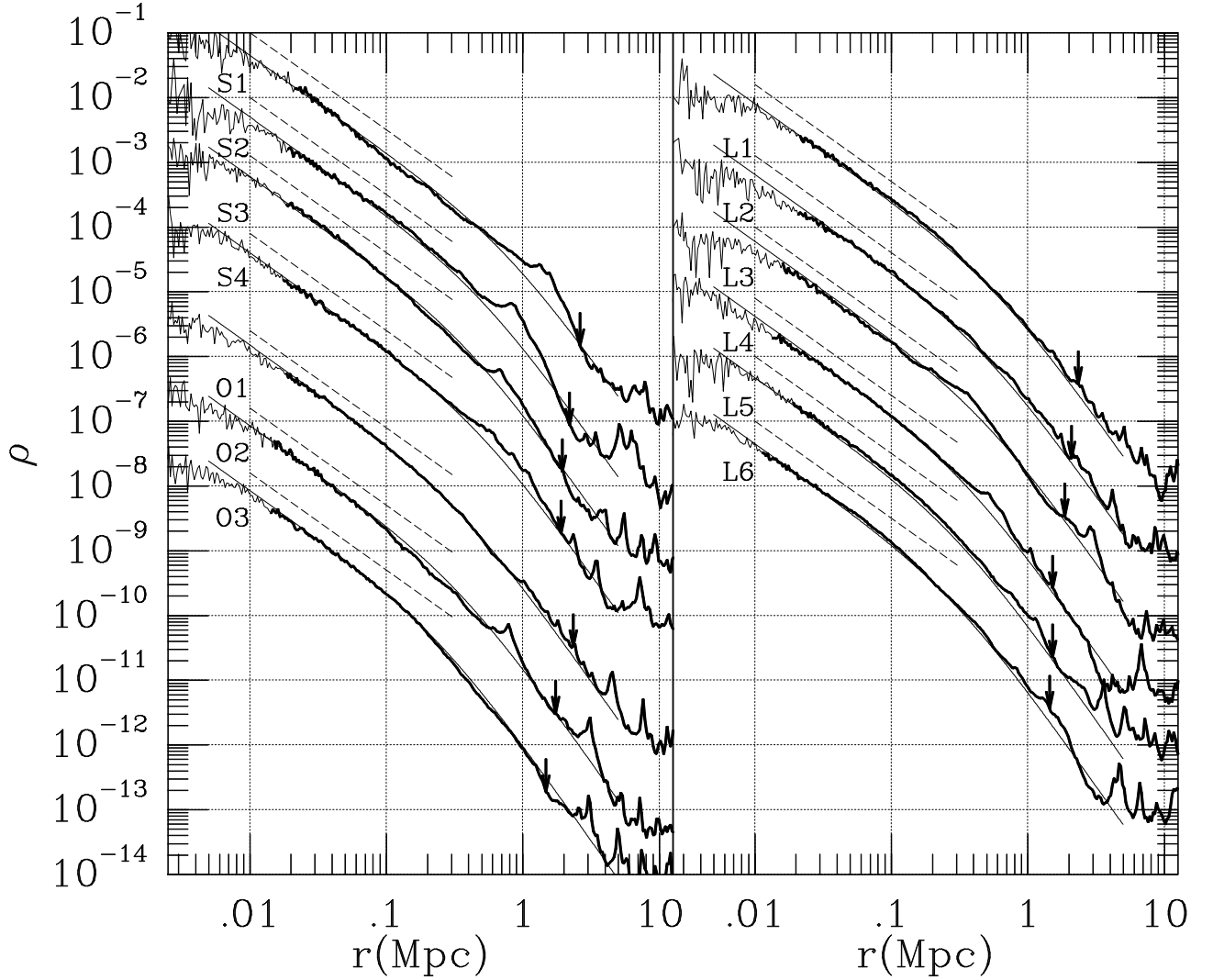


Fig. 2.— Density profiles of the halos for all Runs at  $z \simeq 0$ . Only the densities plotted in the thick lines satisfy the accuracy criteria in section 3.2. Those plotted in the thin lines are influenced by numerical artifacts. The unit of density is  $M_{\odot}/\text{pc}^3$ . The labels on the left of the profiles indicate the run name. The profiles except for Runs S1 are vertically shifted downward by 1, 2, 3, 5, 6, 7 dex for Runs S2, S3, S4, O1, O2, O3, and by 1...6 for Runs L1...L6, respectively. The arrows indicate  $r_v$ . The thin dashed lines indicate the densities proportional to  $r^{-1.5}$ . The thin solid curves indicate the density profile given by equation (2)(the M99 profile).

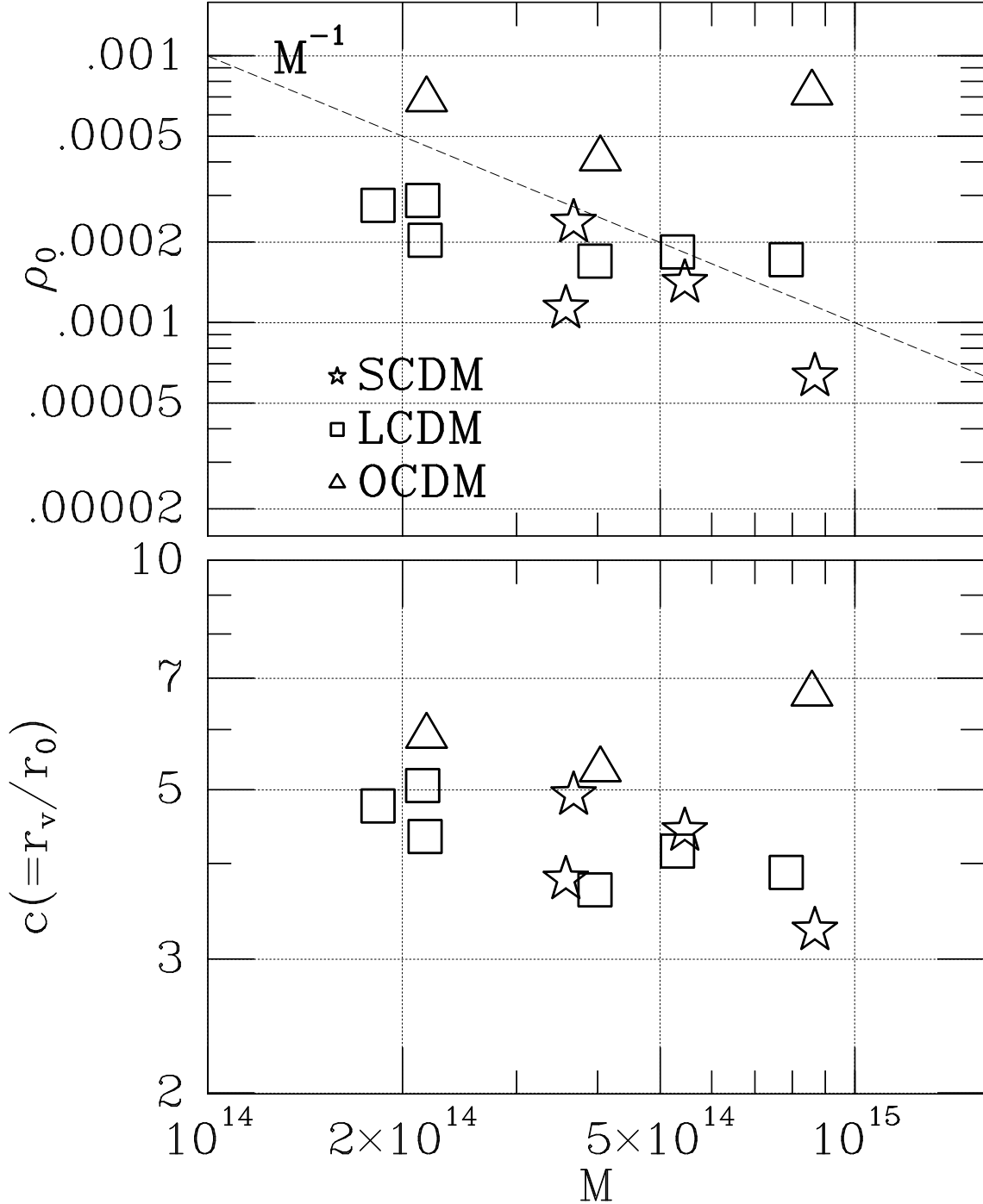


Fig. 3.— Scale density  $\rho_0$  in the unit of  $M_\odot/\text{pc}^3$  and concentration parameter  $c = r_v/r_0$  as a function of total mass in solar mass. The star, square, and triangle symbols show those for SCDM, LCDM, and OCDM models, respectively. The dashed line indicates the self-similar evolutionary track discussed in section 3.3.

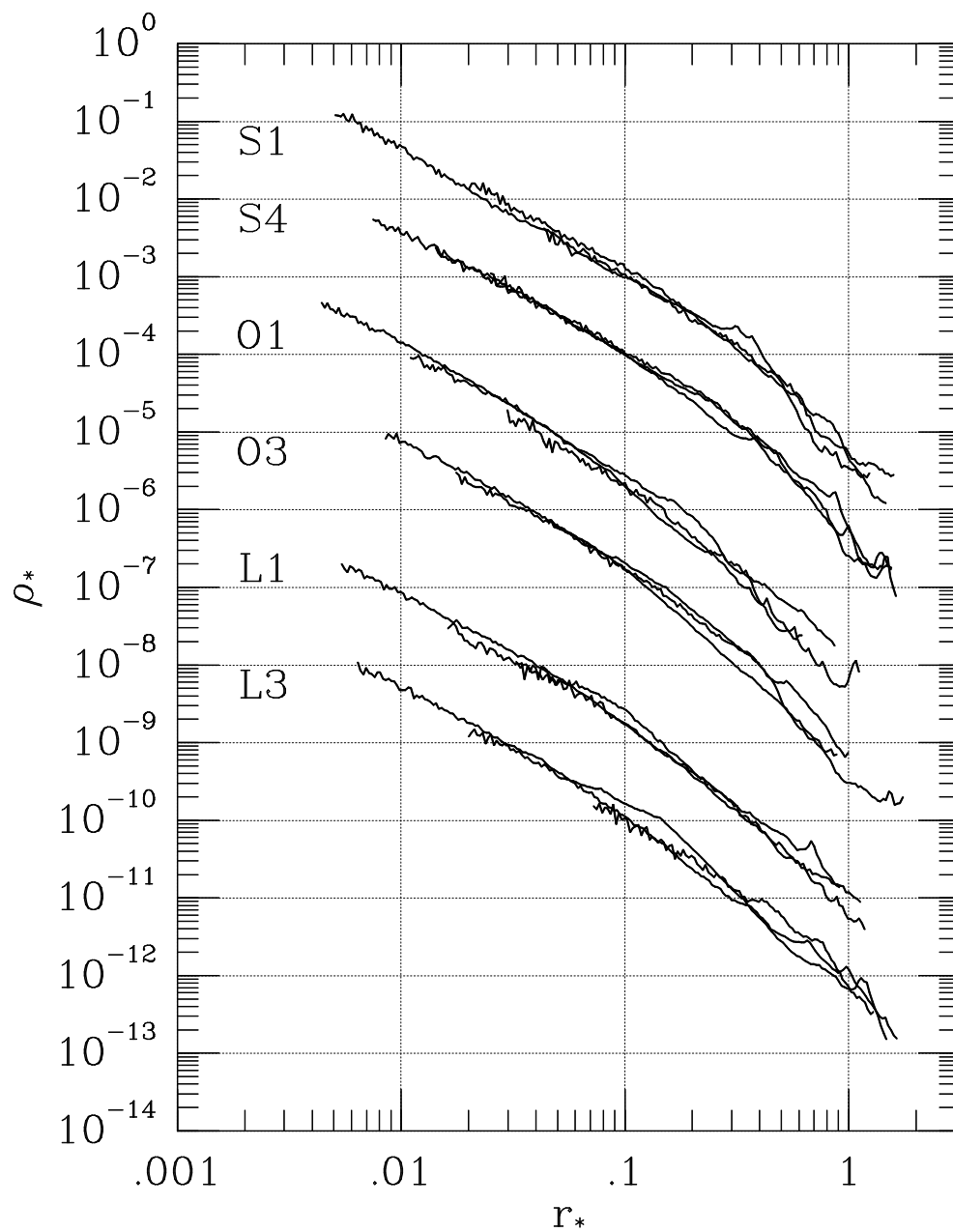


Fig. 4.— Self-similar evolution of the density profile. The scaled densities  $\rho_*$  are plotted as a function of the scaled radius  $r_*$ . The profile for Run S4, O1, O3, L1 and L3 are vertically shifted downward by 1, 3, 4, 6, and 7 dex, respectively. The densities within  $2r_v$  at each redshift are plotted.

Table 2: Simulation Models

Model	Run	$M_v(M_\odot)$	$r_v$ (Mpc)	$N_v$	$m$ ( $10^8 M_\odot$ )	$\Delta t(10^6 \text{yr})$	$N$
SCDM	S1	$8.67 \times 10^{14}$	2.62	1676525	5.17	1.57	5074432
	S2	$5.46 \times 10^{14}$	2.21	1056312	5.17	1.57	3523844
	S3	$3.68 \times 10^{14}$	1.97	1421930	2.58	1.57	3478480
	S4	$3.58 \times 10^{14}$	1.91	1383674	2.58	1.57	4104120
LCDM	L1	$7.83 \times 10^{14}$	2.34	1288779	6.08	0.82	3624848
	L2	$5.32 \times 10^{14}$	2.08	875058	6.08	1.63	4360512
	L3	$3.97 \times 10^{14}$	1.85	1306187	3.04	0.82	3066944
	L4	$2.17 \times 10^{14}$	1.52	1425526	1.52	0.82	3536640
	L5	$2.15 \times 10^{14}$	1.52	707569	3.04	1.63	2058140
	L6	$1.83 \times 10^{14}$	1.43	1809105	1.01	0.82	5458688
OCDM	O1	$8.58 \times 10^{14}$	2.34	1411523	6.08	0.68	3711232
	O2	$4.27 \times 10^{14}$	1.86	702022	6.08	1.37	1748480
	O3	$2.18 \times 10^{14}$	1.47	717056	3.04	1.37	2148736